Journal of Alloys and Compounds 509 (2011) 9218–9225

Contents lists available at ScienceDirect

Journal of Alloys and Compounds

journal homepage: www.elsevier.com/locate/jallcom

Synthesis and characterization of DL-thioctic acid (DLTA)–Fe_3O_4 nanocomposite

E. Karaoğlu[a], A. Baykal[a,*], H. Erdemi[b], L. Alpsoy[c], H. Sozeri[d]

[a] Department of Chemistry Fatih University, 34500 B.Cekmece-Istanbul, Turkey
[b] Department of Polymer Engineering, Yalova University, 77100 Yalova, Turkey
[c] Department of Biology, Fatih University, 34500 B.Cekmece-Istanbul, Turkey
[d] TUBITAK-UME, National Metrology Institute, PO Box 54, 41470 Gebze-Kocaeli, Turkey

ARTICLE INFO

Article history:
Received 7 March 2011
Received in revised form 26 June 2011
Accepted 30 June 2011
Available online 7 July 2011

Keywords:
Fe_3O_4
Nanocomposite
Surface modification
Magnetic property
DL-Thioctic acid

ABSTRACT

DL-Thioctic acid (DLTA) coated magnetite (Fe_3O_4) NP's have been prepared by the co-precipitation of iron oxide in the presence of DLTA. The product identified as magnetite, which has an average crystallite size of 7 ± 2 nm as estimated from X-ray line profile fitting. Particle size was estimated as 11 ± 1 nm from TEM micrographs. FT-IR analysis showed that the binding of DLTA on the surface of iron oxide is through carboxyl group is bidentate. VSM analysis explained the super-paramagnetic nature of the nanocomposite. TG analysis showed that the 80% of the nanocomposite was DLTA and 10% was Fe_3O_4, respectively. The conductivity measurements displayed the magnetic transition at ~60 °C for DLTA–Fe_3O_4 NPs. Analysis of the conductivities reveals the fact that the a.c. conductivity shows a frequency-dependent behavior while d.c. electrical conductivity is strongly temperature dependent and is classified into two regions over a limited temperature range of up to 120 °C. Toxicity was tested measured by LDH assay.

1. Introduction

Magnetite (Fe_3O_4) is a common magnetic iron oxide that has a cubic inverse spinel structure with fcc close packed oxygen anions and Fe cations occupying interstitial tetrahedral and octahedral sites [1]. Due to its strong magnetic and semiconducting properties, magnetite (Fe_3O_4) is one of the preferred well-known filler materials, which is combined with polymers/nanocomposites to be used as magnetic recording media, and in medical applications [2–7]. Therefore, magnetite has the potential for providing the desired magnetic and electrical properties to the final composite.

Functionalization and modification of the surface of SPION [7–17] with various biocompatible and biodegradable materials has been widely examined in biomedicine fields for cell separation [18], diagnostic magnetic resonance imaging (MRI) [19–21] drug delivery systems (DDS) [22] and vaccine administration [23].

DL-Thioctic acid or DL-alpha-lipoic acid (DLTA) is a low molecular weight dithiol antioxidant that is an important co-factor in multienzyme complexes in the mitochondria. Lipoic acid (LA) is available from the diet, absorbed through the gut and easily passes through the blood–brain barrier. As an antioxidant, LA and its reduced form, dihydrolipoic acid (DHLA) are capable of quenching reactive oxygen and nitrogen species such as hydroxyl radicals, peroxyl radicals, superoxide, hypochlorous acid and peroxynitrite and chelating metals such as Cd^{2+}, Fe^{3+}, Cu^{2+} and Zn^{2+} [24,25].

Inorganic nanoparticles coated with conducting polymer to form core/shell structured materials has been demonstrated to be an effective strategy to enhance the stability of composites and widen the applications because of the strong electronic interaction between the inorganic core and polymer shell [26].

The transport property (electronic/dielectric) properties of DLTA–Fe_3O_4 have been rarely reported. To our knowledge, this is the first report on the synthesis and characterization of DLTA–Fe_3O_4 nanocomposite.

2. Experimental

2.1. Chemicals

All chemicals ($FeCl_3 \cdot 2H_2O$, $FeCl_2 \cdot 4H_2O$, DL-Thioctic acid (DLTA)) were obtained from Merck and used without further purification. Lactate dehydrogenase (LDH) and WST-I Cell Proliferation kits were purchased from Roche (Basel, Switzerland). Fetal bovine serum (sigma), RPMI-1640, penicillin/streptomycin, and L-glutamine were purchased from Invitrogen (Paisley, UK).

* Corresponding author. Tel.: +90 212 866 33 00/2061; fax: +90 212 866 34 02.
E-mail address: hbaykal@fatih.edu.tr (A. Baykal).

0925-8388/$ – see front matter © 2011 Elsevier B.V. All rights reserved.
doi:10.1016/j.jallcom.2011.06.118

2.2. Instrumentation

X-ray powder diffraction (XRD) analysis was conducted on a Rigaku Smart Lab Diffractometer operated at 40 kV and 35 mA using Cu K_α radiation.

Transmission electron microscopy (TEM) analysis was performed using a FEI Tecnai G2 Sphera microscope. A drop of diluted sample in alcohol was dripped on a TEM grid.

Fourier transform infrared (FT-IR) spectra were recorded in transmission mode with a Perkin Elmer BX FT-IR infrared spectrometer. The powder samples were ground with KBr and compressed into a pellet. FT-IR spectra in the range 4000–400 cm^{-1} were recorded in order to investigate the nature of the chemical bonds formed.

The real (ε') and imaginary (ε'') parts of complex dielectric permittivity $\varepsilon * [= \varepsilon'(\omega) + i\varepsilon''(\omega)]$ were measured with a Novocontrol dielectric-impedance analyzer. The dielectric data (ε' and ε'') were collected during heating as a function of frequency. The films were sandwiched between gold blocking electrodes and the conductivities were measured in the frequency range 0.1 Hz to 3 MHz at 10 °C intervals. The temperature was controlled with a Novocontrol cryosystem, which is applicable between 20 and 120 °C.

VSM measurements were performed by using a Vibrating sample magnetometer (LDJ Electronics Inc., Model 9600). The magnetization measurements were carried out in an external field up to 15 kOe at room temperature.

The thermal stability was determined by thermogravimetric analysis (TGA, Perkin Elmer Instruments model, STA 6000). The TGA thermograms were recorded for 5 mg of powder sample at a heating rate of 10 °C/min in the temperature range of 30–800 °C under nitrogen atmosphere.

2.3. Procedure

2.3.1. Synthesis of nanocomposite

To an aqueous solution of a mixture of Fe(III) and Fe(II) salts, DL-Thioctic acid solution in the molar ratio 2Fe(III):1Fe(II):4 DL-Thioctic acid was added and kept at a constant temperature of 40 °C for 15 min under vigorous stirring. Then a solution of ammonium hydroxide was added until the pH was raised to ~11 at which a black suspension was formed. This suspension was then refluxed at 80 °C for 6 h, under vigorous stirring and Ar gas. DL-Thioctic acid coated iron oxide (DLTA–Fe_3O_4) nanocomposite was separated from the aqueous solution by magnetic decantation, washed with distilled water several times and then dried in an oven overnight.

2.3.2. LDH test

The human lymphocyte cells were isolated from heparinized blood samples by density-gradient centrifugation over Histopaque washed twice with RPMI-1640 and resuspended in RPMI-1640 supplemented with 5% human AB serum, 100 U/ml penicillin/streptomycin and 2 mM L-glutamine. Cellular injury was determined by measuring the LDH released into the cell culture medium. LDH was assayed by measuring the increase of NADH absorbance at 490 nm and at 25 °C, using a Biotek Power Wave XS mode Elisa Reader (Unico, NJ, USA). Human lymphocyte cells at 2×10^6/ml were treated with 0.08, 0.4, 2, 10 and 20 μg/ml DLTA and DLTA coated iron oxide NPs for 24 h, 48 h and 72 h at 37 °C in 5% CO_2. DLTA concentrations were modified according to DLTA physiologic doses [27]. Then, LDH activity released from human lymphocyte cells into the culture medium, which represents cell death, was determined with an LDH kit as described previously [15,28,29]. Triton X 100 was used as a positive control. All measurements were done three times.

3. Results and discussion

3.1. XRD analysis

Phase investigation of the crystalline product was performed by XRD and the diffraction pattern is presented in Fig. 1. The XRD pattern indicates that the product consists of magnetite, Fe_3O_4, and the diffraction peaks are broadened owing to very small crystallite size. All of the observed diffraction peaks are indexed by the cubic structure of Fe_3O_4 (JCPDS no. 19-629) revealing a high phase purity of magnetite. The following reaction is suggested for the formation of magnetite:

$$Fe^{2+}{}_{(aq)} + 2Fe^{3+}{}_{(aq)} + 8OH^-{}_{(aq)} \rightarrow Fe_3O_{4(s)} + 4H_2O$$

The mean size of the crystallites was estimated from the diffraction pattern by line profile fitting method using Eq. (1) given in [30,31]. The line profile, shown in Fig. 1 was fitted for observed six peaks with the following miller indices: (2 2 0), (3 1 1), (4 0 0), (4 2 2), (5 1 1), and (4 4 0). The average crystallite size, D and σ, was obtained as 7 ± 2 nm because of this line profile fitting.

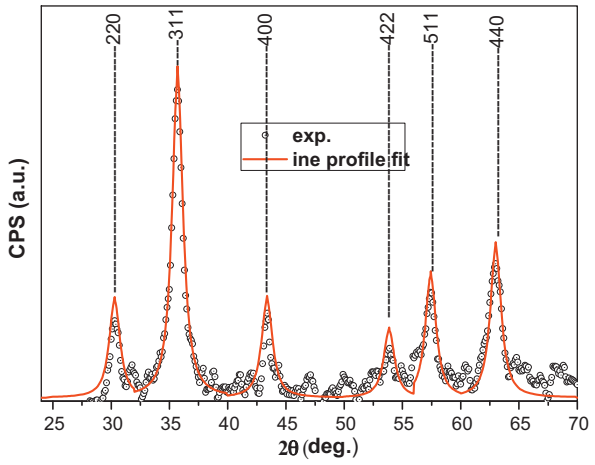

Fig. 1. XRD powder pattern and line profile fitting of DLTA–Fe_3O_4 nanocomposite.

3.2. FT-IR analysis

The structure of DLTA is given in Fig. 2a in which carboxylic acid is clearly visible. FT-IR spectra of Fe_3O_4 NPs, DLTA–Fe_3O_4 nanocomposite, and DLTA along with suggested conjugation scheme of DLTA onto Fe_3O_4 NP's are presented in Fig. 2a–c, respectively. In the spectrum for DLTA presented in Fig. 2c, the strong band at 1700 cm^{-1} could be indicative of the free carboxyl group of DLTA and two sharp bands at 2924 and 2854 cm^{-1} were attributed to asymmetric and symmetric CH_2 stretching vibrations, respectively.

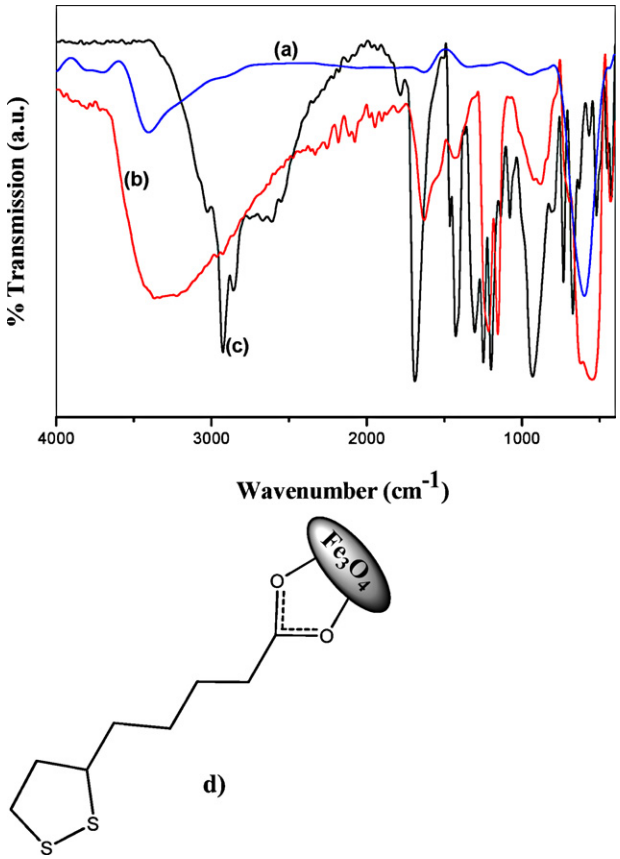

Fig. 2. FTIR spectra of (a) Fe_3O_4 NP's, (b) DLTA–Fe_3O_4 nanocomposite, (c) DLTA, and (d) suggested linkage of DLTA to iron oxide surface.

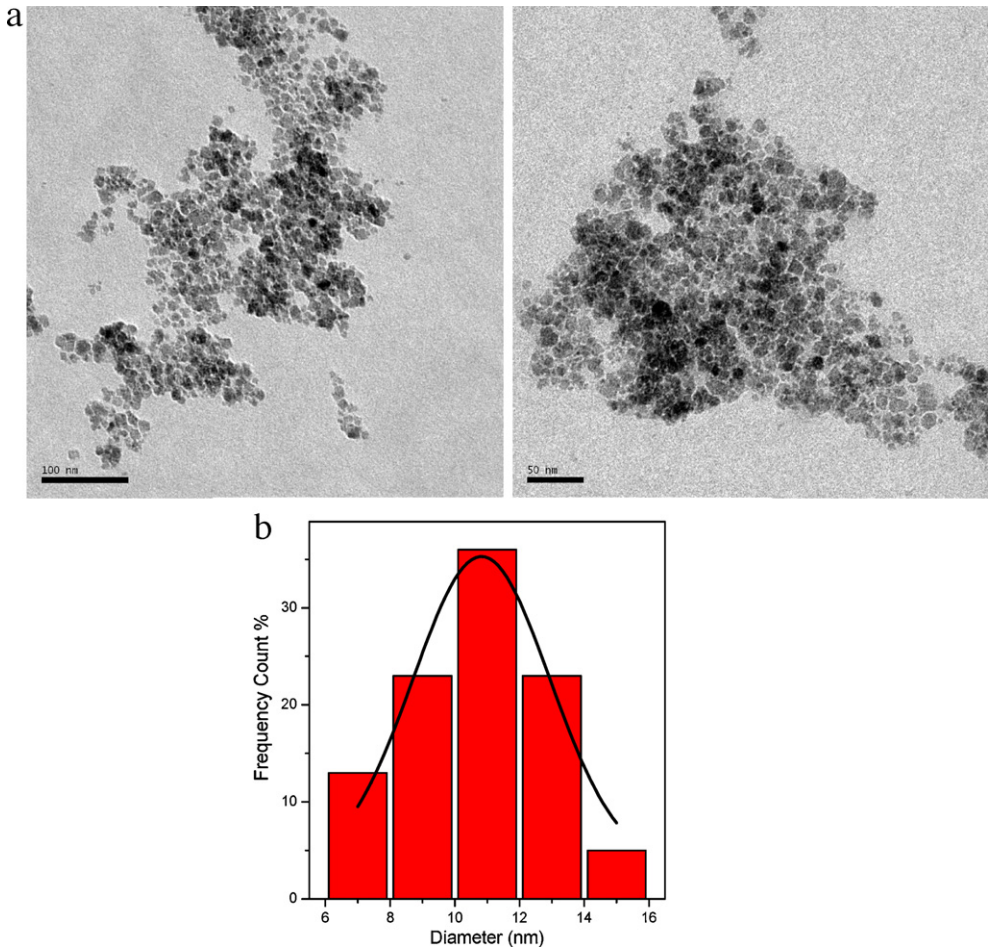

Fig. 3. (a) TEM micrograph of DLTA–Fe_3O_4 nanocomposite and (b) calculated histogram from several TEM images with log-normal fitting.

The intense peak at 1700 cm^{-1} was derived from the existence of the C=O stretch, and the band at 1290 cm^{-1} exhibited the presence of the C–O stretch. It is worth to note that the C=O stretch band of the carboxyl group, which was present at 1700 cm^{-1} in the curve (c), spectrum of the DLTA was absent in the curve (b), spectrum of the coated nanoparticles. In addition, two new bands were observed at 1541 and 1639 cm^{-1}, which were characteristic of the asymmetric ν_{as} (COO^-) and the symmetric ν_s (COO^-) stretch, instead. This result can be explained with the bonding pattern of the carboxylic acids on the surface of the nanoparticle, which was combination of molecules bonded symmetrically and molecules bonded at an angle to the surface [7,14,15,17,32,33]. These results revealed that DLTA were chemisorbed onto the Fe_3O_4 NP's as a carboxylate. The interaction between the carboxylate head and the metal atom was categorized as four types monodentate, bridging (bidentate), chelating (bidentate), and ionic interaction [32,34,35]. According to Zhang et al. [36] the wave number separation, D, between the ν_{as} (COO^-) and ν_s (COO^-) IR bands can be used to distinguish the type of the interaction between the carboxylate head and the metal atom. The largest D (200–320 cm^{-1}) was corresponding to the monodentate interaction and the smallest D (<110 cm^{-1}) was for the chelating bidentate. The medium range D (140–190 cm^{-1}) was for the bridging bidentate [36]. In this study, the D (1625–1547 = 78 cm^{-1}) was ascribed to chelating bidentate, where the interaction between the COO^- group and the Fe atom was covalent (Fig. 2b). The inorganic lattice vibration appears in the range 400–700 cm^{-1}. As prepared powder presents characteristic peaks that are exhibited by the commercial magnetite powder: metal–oxygen band, ν_1, observed at 590 cm^{-1} corresponds to intrinsic stretching vibrations of the metal at tetrahedral site ($Fe_{tetra} \rightarrow O$), whereas metal–oxygen band observed at 445 cm^{-1}; ν_2, is assigned to octahedral-metal stretching ($Fe_{octa} \rightarrow O$) (Fig. 2a) [7,14,15,17,34].

3.3. TEM analysis

The morphology and size distribution of DLTA–Fe_3O_4 nanocomposite was analyzed using TEM. A few micrographs at different magnifications, a histogram calculated thereof are presented in Fig. 3. The Fe_3O_4 nanoparticles exhibit a near spherical morphology at low magnification. The average particle size, calculated by log-normal fitting to the size distribution histogram, obtained was 11 ± 1 nm. As compared with the crystallite size obtained from X-ray line profile fitting, particle size calculated from TEM is larger due to the capping effect [37–39].

3.4. TG analysis

Thermal stability of DLTA and DLTA–Fe_3O_4 nanocomposite was analyzed by TGA and thermograms are presented in Fig. 4a and b, respectively. DLTA shows two-step weight loss behavior (Fig. 4b). The initial weight loss up to 100 °C is due to residual water; second step involves the decomposition of DLTA which started after 250 °C and continued up to 300 °C. DLTA–Fe_3O_4 nanocomposite undergoes similar decomposition steps as that of DLTA, but it has somehow greater stability due to interaction between DLTA and Fe_3O_4. Derivative weight loss (DTG) curves of the DLTA and DLTA–Fe_3O_4

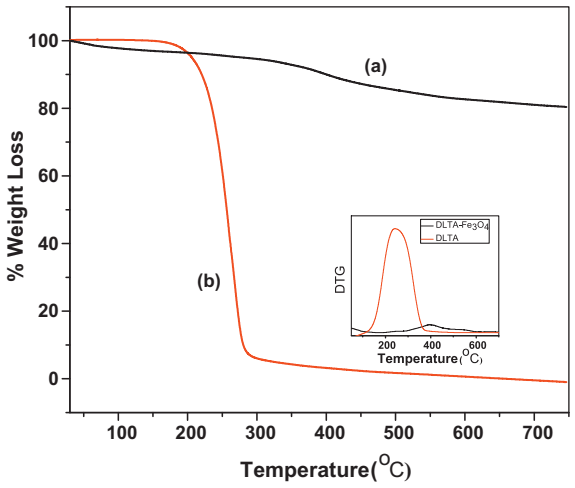

Fig. 4. TGA thermograms of (a) DLTA–Fe_3O_4 nanocomposite and (b) DLTA.

nanocomposite are also illustrated in the inset of Fig. 4. Based on the thermogram, DLTA is 10% of the DLTA–Fe_3O_4 nanocomposite which means an inorganic content is about 80%.

3.5. Magnetic characterization

Room temperature *M–H* hysteresis curve of TDLA-coated magnetite is shown in Fig. 5. It shows the absence of coercivity and remanence. It shows non-hysteric behavior. Besides, magnetization increases with external field and does not saturate up to 15 kOe. These are characteristic features of super-paramagnetic (SP) particles with grain sized less than 20 nm. A saturation magnetization (M_s) value of the nanocomposite is calculated from a plot of *M* vs. $1/H$ (*M* at $1/H \geq 0$) as 49 emu/g, which is considerably lower than that of the bulk magnetite (92 emu/g) [40]. When this M_s value is normalized to the real mass of the magnetite, saturation magnetization becomes 62 emu/g that is still far from the theoretical M_s of this material. Reduced magnetization is generally observed in SP magnetite particles [12,14,41–43] and explained by spin canting together with presence of disordered spins at the surface [12,14,42–44]. As particle size decreases, effect of surface spins to the overall magnetization increases due to the presence of a considerably high fraction of all spins on the surface. Other than these two effects, adsorption of surfactant molecules to the surface of magnetite particles can be another reason of the low magnetization values in the nanocomposites. When magnetite is coated with DLTA, adsorption of surfactant molecules occurs through oxygen atoms that is observed from the FT-IR analysis, see Fig. 2d. As a result, some of the spins of the oxygen atoms, close to the surface, are pinned and do not contribute to the magnetization of the composite. This pinning also weakens the super exchange interaction between Fe–O–Fe atoms, thus, overall magnetization of the nanocomposite decreases further.

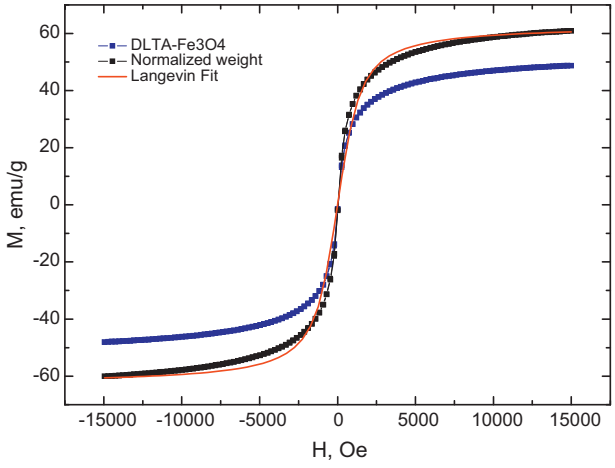

Fig. 5. Room temperature *M–H* curve for DLTA–Fe_3O_4 nanocomposite.

It is also possible to calculate the average particle size of the magnetite using the room temperature M-H hysteresis curve by assuming that they are weakly or non-interacting SP particles. Magnetization of SP particles can be described by the Langevin function which should be fit to the experimental data. Then, mean magnetic moment (μ) of particles is found to determine average particle size (D). Langevin function was fitted to the *M–H* curve of the composite material that is normalize to the mass of magnetite and mean magnetic moment was determined as 7786 μ_B. This is inserted in $\mu = M_s \pi \rho D^3/6$, where ρ is the density of the magnetite particles $\approx$5.18 g/cm^3, and average particle sizes are found to be 7.65 ± 2.00 nm. This agrees well with the particle sizes determined from XRD patterns within the given uncertainities.

3.6. Temperature and frequency dependent conductivity and dielectric permittivity measurements

3.6.1. Conductivity

It is essential to describe the behavior of the nanocomposites under different temperatures in order to understand the conductivity characteristics of this nanocomposite sample. The physical characteristics of nanocomposites such as density and orientation of the organic particles are considerably varied with temperature depending on the nanoparticle content in nanocomposite materials. The low density and random orientations of organic nanoparticles in pure samples give rise to weak connecting among the polymeric nanostructures through the boundaries of nanocrystallites those results in relatively low conductivity. In nanocomposite samples, the organic samples grow on Fe_3O_4 nanoparticle leading to diverse grainy nature as well. Therefore, an enhancement of the density of the composite materials is obtained. With increase in the content of magnetite nanoparticles, the links between the crystallites of the conducting organic nanoparticles are improved since the density in the samples increases. Consequently, the coupling through the crystallite boundaries becomes stronger which eventually brings about the improvement of the macroscopic conductivity measured in the nanocomposite structure.

In the beginning, the magnetite nanoparticles surrounded by DLTA form a random network at low temperatures, and when temperature is increased regularly, nanocomposites become more organized. This phenomenon is described as a formation of the temperature-assisted nanolattice which results in the change of overall conductivity with temperature because of reorganization of temperature related boundings between magnetite and DLTA.

3.6.2. a.c. conductivity

The a.c. conductivities, $\sigma_{ac}(\omega)$ of Fe_3O_4 NPs and DLTA–Fe_3O_4 nanocomposite as a function of frequency and temperature are displayed in Fig. 6a and b. Frequency dependent a.c. conductivities, $\sigma_{ac}(\omega)$, have been derived using the equation [1]:

$$\sigma'(\omega) = \sigma_{ac}(\omega) = \varepsilon''(\omega)\omega\varepsilon_0$$

where $\sigma'(\omega)$ is the real part of conductivity, ω (=$2\pi f$) is the angular frequency ε'' is the imaginary part of complex dielectric permittivity (ε^*) and ε_0 (=8.852×10^{-14} F cm^{-1}) is the vacuum permittivity. Fig. 6a shows that the curves of a.c. conductivity of Fe_3O_4 NPs increases regularly with temperature and does not show

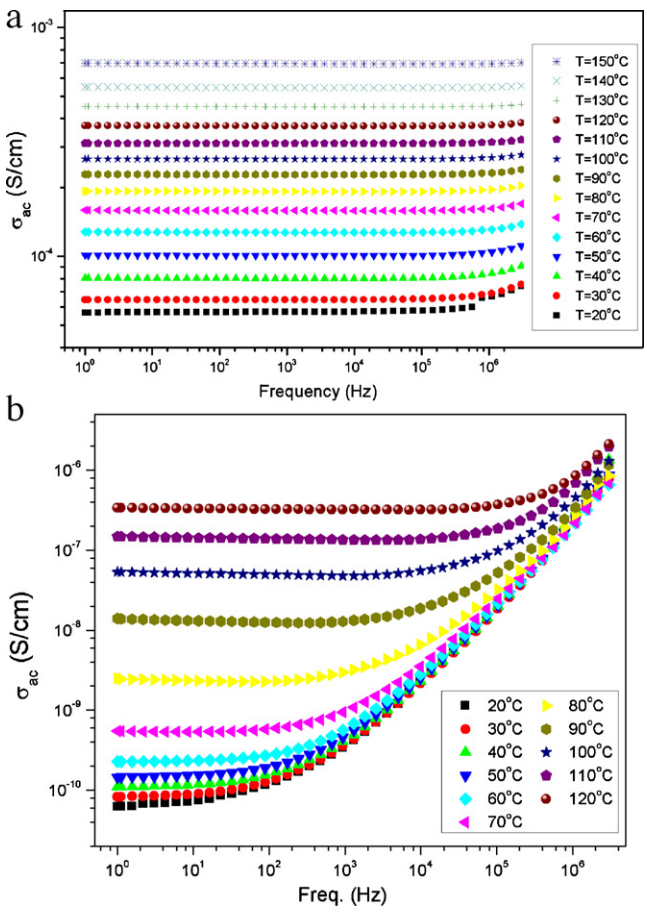

Fig. 6. (a) The a.c. conductivity versus frequency dependence for Fe_3O_4 at various temperatures. (b) The a.c. conductivity versus frequency dependence for DLTA–Fe_3O_4 nanocomposite at various temperatures.

dependency on frequency particularly at lower frequency regime whereas it is strongly temperature dependent and varies in the order of $10^{-4.25}$ to $10^{-3.25}$ S/cm.

The a.c. conductivity of DLTA–Fe_3O_4 nanocomposite versus frequency for various temperatures comprises well-developed conductivity plateau regions. The plateaus start at 1 kHz and shift to higher frequencies up to 100 kHz at high temperatures (Fig. 6b). A significant increase is observed at higher frequencies at all temperature ranges which is assigned to the 'normal' dispersion in polymers [45]. The σ_{ac} increases rapidly with almost equivalent slope as temperature increases but it becomes more apparent and separated above phase transition temperature of about 60 °C which also corresponds to the melting temperature of the pure DLTA. Such a dramatic increase in a.c. conductivity at this temperature can be described by the contribution of the local dynamics, hydrodynamic transport and percolation of the nanocomposites [46]. The small irregularities at low frequency zone and in low temperature region are due to the blocking electrode polarizations and reorganization of the nanoparticles over a phase transition temperature that is consistent with previously reported similar systems [12,13,17].

A comparison between the conductivities of the Fe_3O_4 and DLTA–Fe_3O_4 nanocomposites shows that the composites have lower conductivity. The free surface charge in the medium may decrease due to the surface bonding between Fe_3O_4 and DLTA that results in a lower conductivity. The reason for the observation of frequency-independent plateau at low frequency regime of about less than 10 kHz and at temperatures over 60 °C is the percolation of magnetite across DLTA coated magnetite nanocomposites. The decrease in a.c. conductivity at temperatures below 60 °C and at frequencies below 1 kHz is due to a lack of a percolated magnetite path. As a result, the overall nanocomposite conductivity is mainly due to the contribution of very low a.c. conductivity of DLTA in this frequency range, which constantly decreases with frequency. At the same time, the conductivity at temperatures above 60 °C remains constant or slightly shifts to a threshold frequency of 10 kHz or increases regularly over a frequency of 1 MHz for all temperature ranges which results from the weakness of the frequency response on hopping conduction.

The nanocomposite network response assembles to a well-defined region at low temperatures between frequency 1 Hz and 1 kHz. In this region, the current flows through both the semiconducting-like magnetite and dielectric-like DLTA. The arrangement of the magnetite NPs and dielectrics such as DLTA in individual nanocomposite network is less important since current flows through all the components that result in a network independent response [17,47]. The a.c. conductivity of nanocomposites begins to increase linearly in log–log plots with frequency region above 1 kHz ($T < 70$ °C), due to the increases of conductivity of the DLTA coated magnetite at low temperature while the changes are smaller as temperature increases. It shows that a.c. conductivity of the capacitive component of the nanocomposite is much higher than that of the semiconducting magnetite. Consequently, the conductivity shows a frequency-dependent behavior that is determined by the magnetite connected via high conductivity of the capacitive component in nanocomposite. There is substantial change in the realization of distribution of the nanocomposite since the low and high frequency response is determined by the random magnetite distribution in the nanocomposite. The conductivity of the nanocomposites should increase continuously with frequency if a percolated path of DLTA across the nanocomposite is present.

3.6.3. d.c. conductivity

The d.c. conductivities of Fe_3O_4, DLTA and DLTA–Fe_3O_4 nanocomposite versus reciprocal temperature are displayed in Fig. 7. The frequency independent conductivity is identified with the d.c. conductivity (σ_{dc}) which was derived obtained from the well-developed plateau region in graphs of σ_{ac} vs. Freq. by linear fittings. In non-plateau regions, the middle region was fitted linearly to reduce the effect of electrode polarization and dispersion.

In magnetite nanocomposites, the major conduction takes place by hopping process since ionic or vacant sites charge carriers provide low mobility systems like ferrites. Electron hopping occurs between the neighboring iron cations with two and three valence. In this process, drift mobility of charge carriers increases by increasing temperature resulting an increase in d.c. conductivity. The influence of a number of parameters such as porosity, chemical composition and particle size and cation distribution on the conductivity of magnetite has been discussed in previous reports [48–50].

The d.c. conductivity curves exhibits significant influence of temperature on conductivity involving a transition region. The d.c. curves of magnetite increases regularly with temperature showing no transition as a result single activation energy is identified whereas DLTA–Fe_3O_4 nanocomposite shows a transition over 60 °C providing two values of the activation energies below and above transition temperature. It is clear that this transition temperature is strongly associated with melting temperature of DLTA. Therefore, the transition above 60 °C can be attributed to both magnetic transformation of Fe_3O_4 and melting of the polymer-like organic component that has been already discussed in literature [51]. It has been reported that the single crystals of iron oxide have magnetic transformation in the temperature range of 70–190 °C. The con-

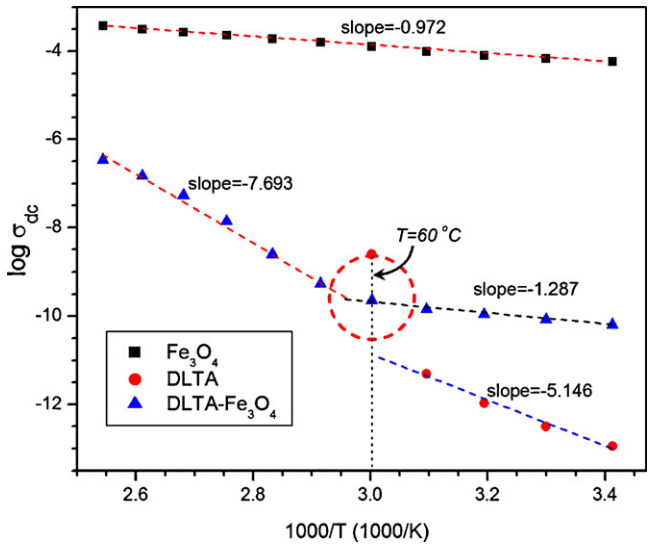

Fig. 7. The d.c. conductivity of (a) Fe_3O_4, (b) DLTA and (c) DLTA–Fe_3O_4 nanocomposite versus reciprocal temperature.

ductivity curves at all temperatures can be fitted with Arrhenius equation as follows:

$$\log \sigma = \log \sigma_0 - \frac{E_a}{kT}$$

where σ_0 and E_a are the pre-exponential term, and the activation energy for each transition region, respectively, and k (=8.617 × 10^{-5} eV K^{-1}) signifies the Boltzmann constant [52]. Two different activation energies (E_a = 1.109 eV and 6.630 eV) were obtained from the slope of the curves for DLTA–Fe_3O_4 nanocomposite before and after transition temperature region. Additionally, the activation energy for DLTA was found to be 4.435 eV. The high activation energy values may explain the reason of having such low d.c. conductivities. The determined activation energy value of magnetite (0.045 eV) is consistent with earlier reported d.c. activation energy [53]. The d.c. conductivity of the nanocomposites in Arrhenius plots represents a regular increment as a function of temperature providing a curvature around transition temperature of 60 °C as shown in Fig. 7c. Complete reorganization of the DLTA capped magnetite NPs occurs over a temperature of 70 °C. As a result, d.c. conductivity increases with the reciprocal temperature up to 60 °C and then a transition region takes place at a temperature range of 60–70 °C. Above 70 °C it increases again rapidly with reciprocal temperature in Arrhenius plot. This behavior is mainly due to the influence of the thermal energy exerted on polymer-like-DLTA at about 60 °C (Fig. 7a and b) [52].

Consequently, the measured electrical conductivity is strongly dependent on temperature and this dependence is often expressed as a slope in logarithmic conductivity versus reciprocal temperature graphs. This behavior is attributed to the temperature-induced transition from 3D, to thermally activated behavior [54]. It should also be emphasized that due to semiconducting nature of magnetite, two different tendencies of activation energy occur around 60 °C, and both obey Arrhenius formulation of $\log \sigma_{dc}$ versus $1/T$ before and after this locality.

3.6.4. Permittivity

The complex permittivity parameters of real ε' and imaginary ε'' parts DLTA–Fe_3O_4 nanocomposites as a function of frequency at various temperature are displayed in Fig. 8a and b, respectively. It is seen that the real part of permittivity of the nanocomposites exhibits a sharp exponential decay with frequency at low temperatures and at low frequency range while it shows a slight decline

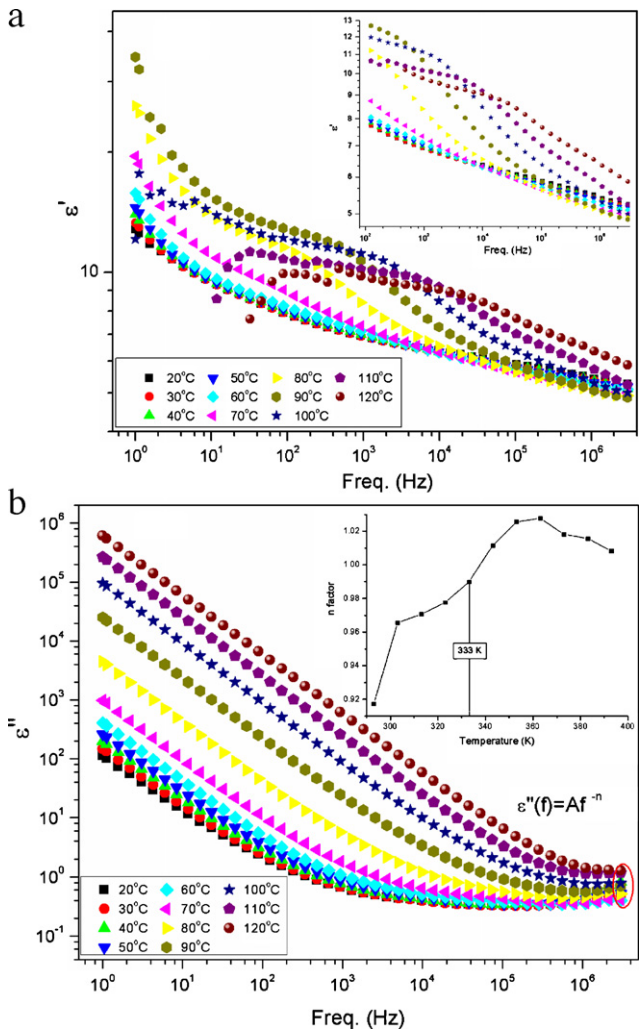

Fig. 8. Real (a) ε' and imaginary (b) ε'' parts of permittivity of DLTA–Fe_3O_4 nanocomposite as a function of frequency at various temperatures.

at high temperatures comprising a curve around 1 kHz over 70 °C. This result is due to the reorganization of nanocomposite at high temperature range as a whole and phase transition when passed through the medium temperature range. It can be also concluded that the variation of the real part of permittivity at high temperatures is less important to some extent in applying external electric field with high frequency.

Imaginary part of the permittivity as a function of frequency for various temperatures was investigated briefly as displayed in Fig. 8b. It represents a linear decrease with frequency which becomes more significant at higher temperatures. This linearity corresponds to the d.c conductivity which is described by the equation $\varepsilon''_{dc} = \sigma_{dc}(\omega C_o)$, where σ_{dc} is the d.c. conductance and C_o is the vacuum capacitance for the unfilled cell in which the electrode plate spacing is equal to the sample thickness [55]. This may also confirm dependency of the conduction mechanism both on temperature and on the nature of the reorganization due to the structural diffusion. It is, however, clear that the capacitive response of the nanocomposites is more temperature dependent rather nature of the reorganization of the DLTA–Fe_3O_4. Additionally, It should be pointed that the conductivity relaxation is predominant over other dielectric relaxations within the given the frequency and temperature since $\varepsilon''_{conduct} \gg \varepsilon''_{relax}$ [56].

The Koop's theory that is based on the Maxwell–Wagner model for the homogeneous double structure may help to explain

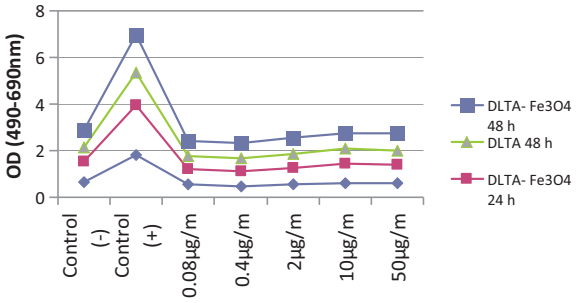

Fig. 9. LDH activity test results for various doses of DLTA, DLTA–Fe_3O_4, positive and negative controls after 24 h and 48 h incubation time period.

the frequency dependent dielectric dispersion curve [57]. In this homogeneous double structure, the highly conducting grains are separated by moderately poor conducting grain boundaries which are found to be more effective at higher frequencies, while grains are more effective at lower frequencies [58]. The conductivity difference between grains and grain boundaries displays different resistances that lead to the accumulation of charge carriers in separated boundaries and enhancement in dielectric constants.

The polarization mechanism in ferrites is similar to the conduction process by electron exchange between Fe^{2+} and Fe^{3+} in which the local displacement of electrons arises in the direction of the applied field determining the polarization. The polarization decreases and reaches to a constant value as the frequency increases because the electron exchange between Fe^{2+} and Fe^{3+} is not as fast as the variation-alternating field. It has been already reported that the large value of dielectric constant at lower frequency is due to the predominance of species like Fe^{2+} ions, oxygen vacancies, grain boundary defects, etc. [59]. This expected result reflects the fact that any species contributing to polarizability is found to exhibit lagging behind the applied field at higher frequencies hence causing a decrease in dielectric constant with frequency [60].

Moreover, the imaginary part of the relative dielectric permittivity of nanocomposite exhibits spectra within the frequency range of measurement which can be analytically wellrepresented by power laws ($\varepsilon''(f) = Af^{-n}$). The inset in Fig. 8b shows the variation of the exponent "*n*" with temperature and the correlated power law exponents are in the range of 0.92–1.03 which is consistent with data reported in the literature [61]. This behavior is also similar for the imaginary part of the permittivity. The observed characteristic nature of the DLTA–Fe_3O_4 nanocomposite seems to be similar to that of its conductivity as shown in previous studies and the inset in Fig. 8b is given for comparison [57]. As seen in Fig. 8b, the imaginary part of permittivity remains unchanged for various temperatures particularly at high frequency range while the exponent "*n*" exhibits linear increase with temperatures up to 60 °C and then it continues to increase linearly with significant change in slope over the transition temperature. This expected result is due to the reorganization of nanocomposite at a certain temperature limit. After complete reorganization of the DLTA capped magnetite NPs the curve achieves a constant value and then begins to decrease as temperature increases further.

Consequently, the dielectric constant increases generally with increasing temperature as seen in semiconductors. The thermal energy converts the bound charges to the charge carriers. The increase in charge carrier concentration always results in easy alignment of dipoles in the applied a.c. electrical field and accordingly increases in dielectric constants. It should be also noted that the mobility of the charge carriers increases by increasing the temperature because of the increase in thermal energy.

3.7. Toxicity

LDH activity test results for various doses of DLTA, DLTA–Fe_3O_4, positive and negative controls after 24 h and 48 h incubation time-period. According to this activity test both DLTA and DLTA–Fe_3O_4 nanocomposite do not have any toxic effect (Fig. 9).

4. Conclusion

We have successfully synthesized DLTA coated iron oxide nanoparticles and characterized it in detail for composition, microstructure, a.c.–d.c. conductivity performance, and dielectric permittivity. FT-IR study showed that DLTA assessed to be covalently bonded to the iron oxide nanoparticle surface via carboxyl groups. Thermal analysis showed that about 80% of the nanocomposite was Fe_3O_4 and 20% was DLTA. The average particle size obtained from VSM was found to be 7.65 ± 2 nm. This agrees well with the crystallite size and particle size determined from XRD patterns and TEM micrographs within the given uncertainities, respectively. VSM showed the superparamagnetic nature of the nanocomposite. The conductivity measurements revealed semiconductor conduction characteristics, and two trends were observed, as a function of frequency and temperature. Analysis of conductivity and dielectric permittivity functions suggest that the conduction mechanism depends both on temperature and on the nature of the reorganization of the nanocomposite due to the structural diffusion. Permittivity measurements showed increasing dielectric constant with increasing temperature as expected from semiconductors.

Acknowledgements

The authors are thankful to the Fatih University, Research Project Foundation (Contract no: P50020902-2) and TUBITAK (Contract no: 110T487) for financial support of this study.

References

[1] R.M. Cornell, U. Schwertmann, The Iron Oxides: Structure, Properties, Reactions Occurrence and Uses , VCH, New York, 1996, p. 28.
[2] W.J. Liang, M. Bockrath, D. Bozovic, J.H. Hafner, M. Tinkham, H. Park, Nature 411 (2001) 665.
[3] V.P. Torchilin, Eur. J. Pharm. Sci. 11 (2000) 81.
[4] L.J. Jeanneret, F. Schmitt, Res. Rev. 27 (2007) 574.
[5] G. Hongwei, X. Keming, Y. Zhimou, C.K. Chang, B. Xu, Chem. Commun. 34 (2005) 4270.
[6] C.V. Mura, M.I. Becker, A. Orellana, D. Wolff, J. Immunol. Methods 260 (2002) 263.
[7] B. Unal, M.S. Toprak, Z. Durmus, H. Sözeri, A. Baykal, J. Nanopart. Res. 12 (2010) 3057.
[8] M. Mikhaylova, D.K. Kim, C.C. Berry, A. Zagorodni, M.S. Toprak, A.S.G. Curtis, M. Muhammed, Chem. Mater. 16 (2004) B2344.
[9] N. Kemikli, H. Kavas, S. Kazan, A. Baykal, R. Ozturk, J. Alloys Compd. 502 (2010) 439.
[10] S. Li, M.M. Lin, M.S. Toprak, D.K. Kim, M. Muhammed, Nano Rev. 1 (2010) 635.
[11] M. Aydın, Z. Durmus, H. Kavas, B. Esat, H. Sözeri, A. Baykal, F. Yılmaz, M.S. Toprak, Polyhedron 30 (2011) 1120.
[12] Z. Durmus, H. Erdemi, A. Aslan, M.S. Toprak, H. Sozeri, A. Baykal, Polyhedron 30 (2011) 419.
[13] Z. Durmus, H. Sözeri, B. Unal, A. Baykal, R. Topkaya, S. Kazan, M.S. Toprak, Polyhedron 30 (2011) 322.
[14] B. Ünal, Z. Durmus, A. Baykal, H. Sözeri, M.S. Toprak, L. Alpsoy, J. Alloys Compd. 505 (2010) 172.
[15] Z. Durmus, H. Kavas, A. Baykal, H. Sozeri, L.S.Ü. Alpsoy, C. elik, M.S. Toprak, J. Alloys Compd. 509 (2011) 2555.
[16] Z. Durmus, H. Kavas, M.S. Toprak, A. Baykal, T.G. Altınçekiç, A. Aslan, A. Bozkurt, S. Coşgun, J. Alloys Compd. 484 (2009) 371.
[17] B. Unal, Z. Durmus, H. Kavas, A. Baykal, M.S. Toprak, Mater. Chem. Phys. 123 (2010) 184.
[18] J. Roger, J. Pons, R. Massart, A. Halbreich, J. Bacri, J. Appl. Phys. 5 (1999) 321.
[19] D. Portet, B. Denizot, E. Rump, J. Lejeune, P. Jallet, J. Colloids Interface Sci. 238 (2001) 37.
[20] P. Wunderbaldinger, L. Josephson, R. Weissleder, Bioconjug. Chem. 13 (2002) 264.

[21] D.K. Kim, Y. Zhang, J. Kehr, T. Klasson, B. Bjelke, M. Muhammed, J. Magn. Magn. Mater. 225 (2001) 256.
[22] S. Gomez-Lopera, R. Plaza, A.V. Delgado, J. Colloids Interface Sci. 240 (2001) 40.
[23] J.J. Kreuter, J. Control. Release 16 (1991) 169.
[24] S. Samuel, R. Kathirvel, T. Jayavelu, P. Chinnakkannu, Toxicol. Lett. 155 (2005) 27.
[25] L. Packer, H.J. Tritschler, K. Wessel, Free Radic. Biol. Med. 22 (1997) 359.
[26] Y. Li, G. Chen, Q. Li, G. Qiua, X. Liu, J. Alloys Compd. 509 (2011) 4104.
[27] K.B. Grogler, G. Niebch, E. Schneider, Eur. J. Pharm. Sci. 8 (1999) 57.
[28] Q. Li, M. Kobayashi, T. Kawada, Toxicology 255 (2009) 53.
[29] K. Yao, D. Huang, B. Xu, N. Wang, Y. Wang, S. Bi, Analyst 135 (2010) 116.
[30] T. Wejrzanowski, R. Pielaszek, A. Opalińska, H. Matysiak, W. Lojkowski, K.J. Kurzydlowski, Appl. Surf. Sci. 253 (2006) 204.
[31] R. Pielaszek, Appl. Crystallography Proceedings of the XIX Conference, Krakow, Poland, 2003, p. 43.
[32] K. Nakamoto, Infrared and Raman Spectra of Inorganic and Coordination Compounds , John Wiley & Son, New York, 1997.
[33] Y.T. Tao, J. Am. Chem. Soc. 115 (1993) 4350.
[34] T. Özkaya, M.S. Toprak, A. Baykal, H. Kavas, Y. Köseoğlu, B. Aktaş, J. Alloys Compd. 472 (2009) 18.
[35] Y. Ren, K. Iimura, T. Kato, Langmuir 17 (2001) 2688.
[36] L. Zhang, R. He, H.C. Gu, Appl. Surf. Sci. 253 (2006) 2611.
[37] K. Uzun, E. Cevik, M. Senel, H. Sozeri, A. Baykal, M.F. Abasıyanık, M.S. Toprak, J. Nanopart. Res. 12 (2010) 3057.
[38] A. Baykal, N. Bıtrak, B. Unal, H. Kavas, Z. Durmus, S. Ozden, M.S. Toprak, J. Alloys Compd. 502 (2010) 199.
[39] Z. Durmus, Synthesis and Characterization of Coated Magnetic Spinel Nanoparticles, Master Thesis, Fatih Univ, İstanbul, Turkey, 2009.
[40] B.D. Cullity, Introduction to Magnetic Materials, vol. 61 , Addison-Wesley, Reading, MA, 1972, p. 190.
[41] J. Mürbe, A. Rechtenbach, T. Töpfer, Mater. Chem. Phys. 110 (2008) 426.
[42] R.H. Kodama, A.E. Berkowitz, E.J. McNiff Jr., S. Foner, Phys. Rev. Lett. 77 (1996) 394.
[43] X. Batlle, A. Labarta, J. Phys. D: Appl. Phys. 35 (2002) R15.
[44] A.E. Berkowitz, J.A. Lahut, I.S. Jacobs, L.M. Levinson, D.W. Forester, Phys. Rev. Lett. 34 (1975) 594.
[45] (a) N.G. McCrum, B.E. Read, G. Williams, Anelastic and Dielectric Effects in Polymeric Solids , Dover, New York, 1991;
(b) D. Kreuer, Solid State Ionics 94 (1997) 55.
[46] M.F.H. Schuster, W.H. Meyer, G. Wegner, H.G. Herz, M. Ise, M. Schuster, K.D. Kreuer, J. Maier, Solid State Ionics 145 (2001) 85.
[47] D.P. Almond, B. Vaines, J. Phys. Condens. Matter 11 (1999) 9081.
[48] E.J.W. Verway, P.W. Haayman, Physica 8 (1941) 979.
[49] V.L.G. Uitert, Proceedings of the IRE, vol. 44, 1956, p. 1294.
[50] R.K. Puri, V. Sayen, Proceedings of the ICF-5, India, 1989, p. 245.
[51] H. Watanabe, N. Tsuya, Sci. Rep. Res. Inst. Tohoku Univ. Ser. A Phys. Chem. Metall. 2 (1950) 29.
[52] S.U. Celik, A. Bozkurt, Eur. Polym. J. 44 (2008) 213.
[53] S. Dutta, S.K. Manik, M. Pal, S.K. Pradhan, C.P.D. Brahma, J. Magn. Magn. Mater. 288 (2005) 301.
[54] M. Okutan, H.I. Bakan, K. Korkmaz, F. Yakuphanoglu, Phys. B: Condens. Matter 355 (2005) 176.
[55] N.G. McCrum, B.E. Read, G. Williams, Anelastic and Dielectric Effects in Polymeric Solids , Dover, New York, 1991, p. 308.
[56] A. Bozkurt, J. Phys. Chem. Solids 63 (2002) 685.
[57] A.M.M. Farea, S. Kumar, K.M. Batoo, J. Alloys Compd. 464 (2008) 361.
[58] K.M. Batoo, S. Kumar, C.G. Lee, Curr. Appl. Phys. 9 (2009) 1397.
[59] G. Bidan, O. Jarjayes, J.M. Fruchart, E. Hannecart, Adv. Mater. 37 (1989) 289.
[60] M.X. Wan, J.C. Li, Polym. Sci. Part A: Polym. Chem. 36 (1998) 2749.
[61] C. Brosseau, P. Talbot, IEEE Trans. Dielectr. Electr. Insulat. 11 (2004) 819.